Combined Sizing and Energy Management in EVs With Batteries and Supercapacitors

Rui Esteves Araújo, *Member, IEEE*, Ricardo de Castro, *Member, IEEE*, Cláudio Pinto, *Student Member, IEEE*, Pedro Melo, *Student Member, IEEE*, and Diamantino Freitas

***Abstract*—This paper is concerned with the study of combined sizing and energy management algorithms for electric vehicles (EVs) endowed with batteries and supercapacitors (SCs). The main goal is to find the number of cells of each source that minimizes the installation and running costs of the EV, taking into account the performance requirements specified for the vehicle and the technical constraints of the energy sources. To tackle this problem, two methodologies will be investigated. The first considers a filter-based approach to perform the power split among the sources; it will be shown that, under some practical assumptions, the resultant sizing problem can be posed as a linear programming problem and solved using efficient numerical techniques. The second methodology employs an optimal noncausal energy management, which, when integrated with the sizing problem, yields a nonlinear optimization problem. These two methodologies will be then applied to size the storage unit of a small EV. The results indicate that the filter-based approach, although simple and numerically efficient, generally requires an oversized storage unit. Furthermore, it was also concluded that, if the range requirements of the EV are not very high (below 50 km, in our case study), the use of SCs enables energy savings of up to 7.8%.**

***Index Terms*—Batteries, electric vehicles, hybrid energy storage system, supercapacitors, sizing.**

I. Introduction

In spite of the environmental benefits provided by electric vehicles (EVs), the main obstacle to the affirmation of electric propulsion still lies in the energy storage system (ESS). The success of this new transportation option will only be achieved if the ESS offers sound features, such as long life cycle, reasonable cost, fast charge times, and high power and energy densities [1]. However, given the current state of technology, these features are difficult to combine into a single class of storage and remain distant from the energy capacity offered by internal-combustion-engine-based vehicles. For instance, batteries, even taking into account the most recent Li-ion chemistries, are generally bulky and relatively expensive, and withstand a limited number of charges/discharges [2]. Although they remain the most popular choice for the ESS of pure EVs, the specific energy (in watthours per kilogram) of today's batteries is still, roughly, 100 times lower than gasoline [3], which poses important constraints on the driving range of the vehicle. Alternatively, supercapacitors (SCs) support a much larger number of charge/discharge cycles and have a good ability to cope with high current peaks, due to their reduced energy losses, but the very low energy density hampers their cause [4]. Fuel cells (FCs) are another attractive energy source but suffer from the limited ability to satisfy power peaks and are still at an early stage of commercial development, facing many practical challenges associated with hydrogen storage and refuelling [5].

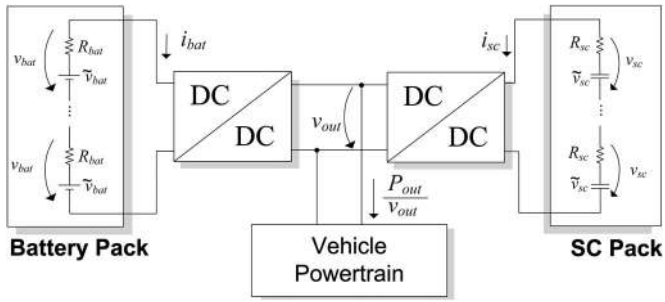

Fig. 1. Block diagram of the HESS considered in this paper.

Consequently, in the absence of an ideal power source, several energy source hybridization strategies have been proposed in the literature [4], [6]–[8], which are driven by the idea of combining storage technologies with complement features. As pointed out by [2] and [4], in the majority of these hybridizations, there is main energy storage with relatively high energy capabilities (e.g., FC or batteries), which is aided by a peaking power source (e.g., SCs). This combination generally leads to a stress reduction in the main source [9], which contributes to its lifetime extension. In addition, due to the low energy losses of the peak power source, the energy efficiency is also increased [10].

This paper is concerned with the hybridization of batteries and SCs, connected to the dc bus through an active parallel arrangement (see Fig. 1). More specifically, the main goal is to investigate how the SCs and batteries should be sized to:

Manuscript received September 1, 2013; revised January 12, 2014; accepted March 16, 2014. Date of publication April 17, 2014; date of current version September 11, 2014. This work was supported in part by the Science and Technology Foundation of Portugal under Scholarship Grant SFRH/BD/47882/2008. The review of this paper was coordinated by Dr. A. Davoudi.

R. E. Araújo and C. Pinto are with the INESC TEC (formerly INESC Porto), Faculty of Engineering, University of Porto, Rua Dr. Roberto Frias, Porto 4200-465, Portugal (e-mail: raraujo@fe.up.pt; ee07317@fe.up.pt).

R. de Castro is with the Institute of System Dynamics and Control, German Aerospace Center, Wessling 82234, Germany (e-mail: Ricardo.DeCastro@dlr.de).

P. Melo is with the Faculty of Engineering, University of Porto, Rua Dr. Roberto Frias, Porto 4200-465, Portugal, and also with the Polytechnic Institute of Porto, Porto 4200-072, Portugal (e-mail: pma@isep.ipp.pt).

D. Freitas is with the Department of Electrical and Computer Engineering, Faculty of Engineering, University of Porto, Rua Dr. Roberto Frias, Porto 4200-465, Portugal (e-mail: dfreitas@fe.up.pt).

Color versions of one or more of the figures in this paper are available online at http://ieeexplore.ieee.org.

Digital Object Identifier 10.1109/TVT.2014.2318275

1) provide enough power and energy to fulfill the EV specifications, such as the range, maximum speed and acceleration, climbing capabilities, etc., and 2) explore the complementary features of the sources to optimize a given performance index, such as the installation costs, energy efficiency, or battery degradation. For ESS composed of a single source, it is, in general, not too difficult to size the storage unit capable of fulfilling these fundamental requirements. For instance, in battery-powered EVs, we can easily pick a minimum battery pack that is able to provide the necessary energy and peak power required by the vehicle. However, for an ESS composed of more than one source, i.e., a hybrid ESS (HESS), the selection process is not that straightforward because the operating points of each source are dependent on how the power is split among them. In other words, there is interdependence between the energy management algorithm and the sizing task. This matter is further complicated by the different costs, energy efficiencies, degradation properties, and lifetime that each source presents. Notice that, while the energy management for the hybridization of batteries and SCs has been widely investigated in the last few years (see, e.g., [9], [11], and [12]), the sizing task for this particular HESS configuration has received less attention in the literature. In [13]–[15], preliminary studies on the battery–SC sizing task are presented, but these fail to provide an accurate account of the energy losses in the powertrain components and/or ignore the important coupling between the sizing and energy management. With regard to this last factor, recent studies on the design of FC–battery [16], [17], hybrid [18], and plug-in [19] EVs have shown that, to maximize the benefits of hybridization, it is imperative to take into account the coupling between the sizing and the energy management. Accordingly, this paper extends these previous studies by contemplating the combined sizing/energy management problem for the hybridization of batteries and SCs. To gain some insight on this issue, we will start by designing the HESS under the assumption that the power allocation between the sources is performed with a frequency-based strategy, i.e., employ the SCs to handle the high-frequency power peaks, while the batteries provide the low-frequency demands. Despite being simple and numerically efficient, the frequency-based sizing only provides rough estimates. This factor prompted us to develop a second methodology, relying purely on an optimization framework (both for sizing and energy management), which, as will be shown in the latter part of this paper, outperforms the frequency-based approach. A preliminary version of this paper was presented in [20] and is extended here in two directions. First, a detailed energy loss model of the powertrain's components was incorporated in the problem formulation, which contributes to a more realistic sizing setting. Second, the optimization problem was also modified to allow the designer to explore tradeoffs between installations costs and energy efficiency of the HESS.

The remainder of this paper is organized as follows. Section II introduces the mathematical model of the energy sources, the loss model in the powertrain's components, and the power and energy requirements for the sizing problem. The filter-based sizing is given in Section III, which is then followed in Section IV by the optimal-based sizing. These two approaches are then applied in Section V to size the HESS of a small EV. Finally, the conclusions are presented in Section VI.

II. Energy Storage System Model and Requirements

A. Simplified Model for the Cells

As shown in Fig. 1, this paper considers that each energy source in the EV is composed by a string of identical n_j cells, $j \in \{\text{bat, sc}\}$. For each cell, a simplified voltage-resistor model is employed [1]

$$\frac{dQ_j(t)}{dt} = -i_j(t) \quad q_j(t) = \frac{Q_j(t)}{\overline{Q}_j} \tag{1a}$$

$$\tilde{v}_j\left(q_j(t)\right) = a_j + b_j q_j(t) \tag{1b}$$

$$v_j(t) = \tilde{v}_j(t) - R_j i_j(t) \tag{1c}$$

where Q_j represents the cell's charge, $\overline{Q}_j$ represents the maximal charge, and q_j represents the state of charge (SOC). The internal voltage $\tilde{v}_j$ is considered an affine map, with the SOC as input, offset a_j, and gain b_j; the cell's output voltage v_j is obtained by subtracting the voltage drop in R_j (the equivalent internal resistance of the cell). The power delivered by the HESS can be expressed as

$$P_{\text{in}}(t) = P_{\text{bat}}(t) + P_{\text{sc}}(t) = \sum_{j \in \{\text{bat, sc}\}} n_j \tilde{v}_j(t) i_j(t). \tag{2}$$

By integrating this relation, we can determine the energy consumption of the vehicle ($E_{\text{in}} = \int_0^T P_{\text{in}}(t)\,dt$). Although more precise models for the SCs [21] and batteries [22] are available, the simplified representation considered in this paper is a sufficient means to analyze the main energy phenomena, enabling us to gain some insight regarding the optimum sizing and energy management, without introducing unnecessary complexity into the mathematical structure of the problem. In fact, this approach is widely used in the literature related to the energy management of hybrid sources [16], [18], [19], [23].

1) Extraction of the Cell's Parameters: The battery and SCs under consideration here were selected having in mind the hybridization of the energy source of the uCar EV (see [24] for additional details on this vehicle). The selection process of the cells was constrained by a reduced budget and a very limited set of supplier options. These constraints ended up confining our choice to NiMH batteries, based on the cells of the module NHE 10–100 [25] (nominal voltage of 1.2 V, 100 Ah), and the SCs BCAP1500 [26] (1500 F@2.7 V).

The identification of the battery parameters $\hat{\theta}_{\text{bat}} = [\, a_{\text{bat}} \quad b_{\text{bat}} \quad R_{\text{bat}} \,]$ was carried out with the help of a weighted least squares method, which seeks to approximate the cell's discharge curve with the linear model (1). This fitting problem can be defined as

$$\min_{\hat{\theta}_{\text{bat}}} \sum_{k=1}^{N_I} \varrho_k \left(v_{\text{bat}}(t_k) - [\, 1 \quad q_{\text{bat}}(t_k) \quad -i_{\text{bat}}(t_k) \,]\, \hat{\theta}_{\text{bat}} \right)^2 \tag{3}$$

where $v_{\text{bat}}(t_k)$, $q_{\text{bat}}(t_k)$, and $i_{\text{bat}}(t_k)$ are the battery voltage, SOC, and current measures acquired during the discharge test

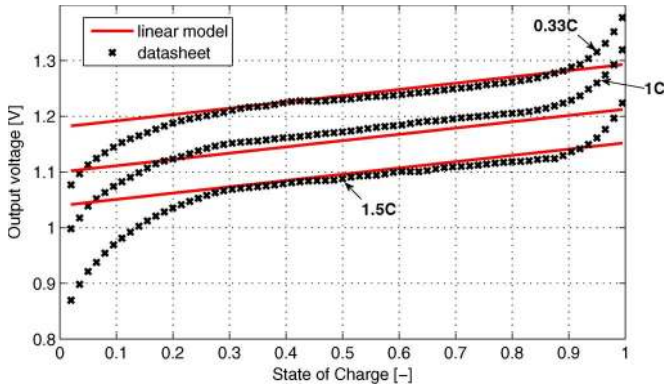

Fig. 2. Discharge curves of the battery cell with nominal temperature and different rates.

of the cell respectively, and N_I is the number of samples. Weight ϱ_k was included in the fitting problem to decrease the contribution of the samples where the nonlinearity effects are more pronounced, i.e., when $q_{\rm bat}$ reaches the operation extremes. Given that the battery under consideration presents an almost linear behavior for $q_{\rm bat} \in [0.2, 0.8]$ (see Fig. 2), weight ϱ_k was selected as

$$\varrho_k = \begin{cases} 1, & \text{if } 0.2 \leq q_{\rm bat}(t_k) \leq 0.8 \\ 0, & \text{otherwise.} \end{cases} \tag{4}$$

As shown in Fig. 2, the identified model obtained with (3) renders a very reasonable approximation for the linear region of the discharge curve, showing a maximum fitting error of only 0.02 V for $q_{\rm bat} \in [0.2, 0.9]$. Notice that, to prevent the early degradation of the cells, it is a common practice to avoid the battery use when $q_{\rm bat}$ is too low/high; therefore, this means that, the linear range aforementioned ends up representing the bulk of the cell's working range.

Regarding the parameters of the SCs, i.e., $\hat{\theta}_{\rm sc} = [\, a_{\rm sc} \quad b_{\rm sc} \quad R_{\rm sc} \,]$, we recall the fundamental relation between the SCs internal voltage, capacitance C and charge

$$\tilde{v}_{\rm sc}(t) = \frac{1}{C} Q_{\rm sc}(t) = \frac{\overline{Q}_{\rm sc}}{C} q_{\rm sc}(t) = \overline{v}_{\rm sc} q_{\rm sc}(t) \tag{5}$$

where $\overline{v}_{\rm sc}$ is the SC voltage when fully charged. Equating the previous relation with (1b), we have $a_{\rm sc} = 0$ and $b_{\rm sc} = \overline{v}_{\rm sc}$; since the nominal SC voltage $\overline{v}_{\rm sc}$ and internal resistance $R_{\rm sc}$ are generally given in the datasheet, parameters $\hat{\theta}_{\rm sc}$ can be straightforwardly determined using the information provided by the SC's manufacturer. The values of $\hat{\theta}_{\rm bat}$ and $\hat{\theta}_{\rm sc}$, together with the cost (c_j) and mass (m_j) per cell, are defined in Table I.

B. Nominal Driving Cycling, Power, and Energy Demand

In terms of vehicle performance specification, the HESS should be designed to satisfy the power and energy demands of a given nominal driving cycle, with speed profile $V(t)$; road angle $\alpha(t)$, $t \in [0, T_{\rm dc}]$; and duration $T_{\rm dc}$. There are two main approaches to characterizing the driving cycle's variables. The first approach follows a stochastic setting and considers that the variables $V(t)$, $\alpha(t)$, $T_{\rm dc}$ have a nonnegligible degree of uncertainty, which can be characterized by probabilistic models, such as the Markov chains [27], [28]. This approach is particularly useful for general-purpose vehicles, where the exact mission profile is not known in advance and is affected by difficult-to-model factors, such as road type, traffic conditions, etc. On the other hand, the second approach regards the driving cycle's variables $V(t)$, $\alpha(t)$, $T_{\rm dc}$ as deterministic, i.e., without uncertainty, and is suitable for vehicles in which the mission has a well-defined pattern. Collection trucks [29], buses [19], mail delivery, and similar vehicles, represent a class of vehicles in which the deterministic approach is acceptable. In this paper, we will assume that the uCar vehicle operates with a well-defined driving cycle, and the HESS will be sized within a deterministic setting. It is also worth pointing out that the typical performance metrics employed at the vehicle design stage, such as top speed, minimum acceleration times, maximum

TABLE I
VEHICLE AND POWERTRAIN PARAMETERS

Variable	Value
vehicle mass (m)	500 kg
rolling resistor coefficient (f_r)	0.013
aero. drag coefficient (C_d)	0.35
vehicle frontal area (A_f)	1.8 m^2
wheel radius (r)	0.3 [m]
sample time T_s	1[s]
cost factor γ	0.11[$/Ws]
cost of a cell, c_{bat}/c_{sc}	95/45 [$]
mass of a cell, m_{bat}/m_{sc}	1.86/0.5 [kg]
resistance of a cell, R_{bat}/R_{sc}	1.2/0.47 [mOhm]
voltage offset, a_{bat}/a_{sc}	1.22/0 [V]
voltage gain, b_{bat}/b_{sc}	0.11/2.70 [V/-]
cell charge, $\overline{Q}_{bat}/\overline{Q}_{sc}$	360/4.0 [kAs]
cell min. SOC, $\underline{q}_{bat}/\underline{q}_{sc}$	0.2/0.5 [-]
cell max. SOC, $\overline{q}_{bat}/\overline{q}_{sc}$	0.90/0.99 [-]
initial SOC, $q_{bat,0}/\ q_{sc,0}$	0.90/0.99 [-]
maximum current, $\overline{i}_{bat}/\overline{i}_{sc}$	300/400 [A]
minimum current, $\underline{i}_{bat}/\underline{i}_{sc}$	-300/-400 [A]
max. RMS current, $\overline{I}_{rms,bat}$	100 [Arms]
max. RMS current, $\overline{I}_{rms,sc}$	140 [Arms]
derating factor, $\overline{\chi}_{bat}/\overline{\chi}_{sc}$	0.9/1 [-]
usable energy of a cell, e_{bat}/e_{sc}	81.5/1.1[Wh]
peak power of a cell, p_{bat}/p_{sc}	273/1080 [W]
estimated energy efficiency, $\hat{\eta}_{PT}$	0.75[(1)]
DC/DC eff. parameter, D_0	270[W]
DC/DC eff. parameter, D_1	32[mOhm]
transmission efficiency, η_{TR}	0.98
Motor losses parameters, $\mathbf{M}^T$	$[144, 0.5, 0, 0.07, 0.36, 0]$
reduction ratio, G	7

(1) estimation based on the expected average efficiency of the powertrain, i.e. $\hat{\eta}_{PT} = f(\mathbf{x}_{avg})/d_\eta$, where $\mathbf{x}_{avg}$ is vector with the average operating point of the vehicle (e.g., average speed, average output power, etc), $f(.)$ the powertrain's efficiency map - calculated from (9) and (10) - and $d_\eta = 1.1$ is a derating factor that brings an additional safety margin to cope with the errors introduced by the constant-efficient approximation.

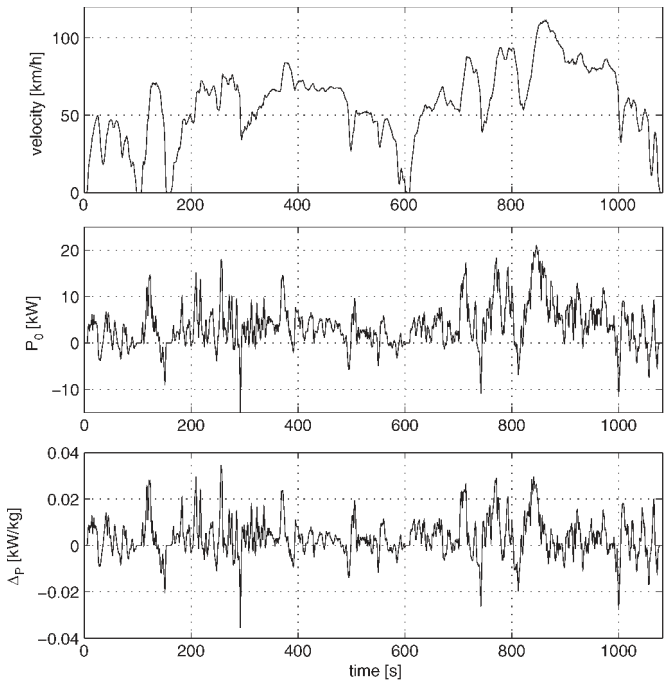

Fig. 3. Velocity and power request associated with the ARTEMIS road cycle (considering $\alpha(t) = 0$), which is regarded as the nominal driving cycle throughout this paper.

gradability, and vehicle range, can be easily incorporated in the $V(t)$ and $\alpha(t)$ profiles.

Using the nominal driving cycle information, together with the application of Newton's law, the power requested to the HESS can be defined as (see [30] for additional details)

$$P_{\rm out}(t) = \underbrace{V(t)\left(\frac{1}{2}\rho_a C_d A_f V(t)^2\right)}_{P_a(t)} + M\underbrace{\left(gf_r\cos(\alpha(t)) + g\sin(\alpha(t)) + \frac{dV(t)}{dt}\right)V(t)}_{\Delta_P(t)} \quad (6)$$

where M is the vehicle total mass, g is the acceleration due to gravity, P_a is the power due to aerodynamic drag, and $M\Delta_P$ is the power due to inertial, grading, and rolling resistance forces (The definition and value of the remaining parameters are presented in Table I).

Since M is also affected by the HESS mass, i.e., $M = m + n_{\rm bat}m_{\rm bat} + n_{\rm sc}m_{\rm sc}$, where m is the vehicle mass without the storage units, $P_{\rm out}$ can be further decomposed into two components, i.e.,

$$\begin{aligned} P_{\rm out}(t) &= \underbrace{P_a(t) + \Delta_P(t)m}_{P_0(t)} + \Delta_P(t)(n_{\rm bat}m_{\rm bat} + n_{\rm sc}m_{\rm sc}) \\ &= P_0(t) + \Delta_P(t)(n_{\rm bat}m_{\rm bat} + n_{\rm sc}m_{\rm sc}) \end{aligned} \quad (7)$$

where $P_0(t)$ (in watts) is the nominal power, and $\Delta_P(t)$ (in watts per kilogram) is the power increase due to the HESS mass. This power decomposition is shown in Fig. 3 for the ARTEMIS road cycle, which is regarded as the nominal driving cycle throughout this paper.

The energy requested to the HESS can be obtained by direct integration of $P_{\rm out}(t)$

$$\begin{aligned} E_{\rm out}(t) &= \underbrace{\int_0^t P_0(s)ds}_{E_0(t)} + (n_{\rm bat}m_{\rm bat} + n_{\rm sc}m_{\rm sc})\underbrace{\int_0^t \Delta_P(s)ds}_{\Delta_E(t)} \\ &= E_0(t) + \Delta_E(t)(n_{\rm bat}m_{\rm bat} + n_{\rm sc}m_{\rm sc}) \end{aligned} \quad (8)$$

where E_0 (in wattseconds) is the nominal energy, and Δ_E (wattseconds per kilogram) is the energy increase due to the HESS mass. Although one may question the need to contemplate the influence of the HESS mass in the power/energy required by the driving cycle, it is important to have in mind that this parameter is unknown at the start of the sizing phase. Furthermore, for light EVs, which is the type of vehicle under consideration here, the HESS represents an important portion of the global vehicle's mass and, as will be shown later on, has a nonnegligible impact on the energy consumption of the EV.

C. Power Losses

The power delivered by the HESS must take into account not only the power required by the driving cycle $P_{\rm out}$ but also the power losses in the powertrain components, such as the transmission $(P_{l,\,\rm TR})$, the electric motor $(P_{l,\,\rm EM})$, the dc/dc converters $(P_{l,\,\rm DCDC})$, and the HESS $(P_{l,\,\rm ESS})$. As a result, the following power balance constraint must be respected:

$$P_{\rm in} = P_{\rm out} + P_l = \begin{cases} P_{\rm out} + P_l, & \text{if } P_{\rm out} \geq 0 \\ -|P_{\rm out}| + P_l, & \text{otherwise} \end{cases} \quad (9)$$

$$P_l = P_{l,\,\rm ESS} + P_{l,\,\rm DCDC} + P_{l,\,\rm EM} + P_{l,\,\rm TR}. \quad (10)$$

Here, a brief review of practical loss model for the powertrain components is presented, targeting its final incorporation in the sizing problem.

Under the assumption that the HESS response can be approximated by the voltage-resistor model presented in (1), the energy losses in this component are given by

$$P_{l,\,\rm ESS}(t) = n_{\rm bat}R_{\rm bat}i_{\rm bat}(t)^2 + n_{\rm sc}R_{\rm sc}i_{\rm sc}(t)^2. \quad (11)$$

Both batteries and SCs are connected to the dc bus via two bidirectional boost converters (see Fig. 1), with identical characteristics. According to [31]–[33], the energy losses in the dc/dc converters (see Fig. 4) are due to: 1) conduction losses in the semiconductors; 2) switching losses; and 3) losses in the passive elements (inductor and capacitor). These three types of losses can be compactly expressed as

$$\begin{aligned} P_{l,\,\rm DCDC}(t) = &\sum_{j\in\{\rm bat,\,sc\}} C_0 + \Big(C_1 + C_2\tilde{d}(v_j(t),\, i_j(t))\Big)|i_j(t)| \\ &+ \Big(C_3 + C_4\tilde{d}\,(v_j(t),\, i_j(t))\Big)\, i_j(t)^2 \\ \tilde{d}(v_j,\, i_j) = &\begin{cases} 1 - \frac{v_j}{v_{\rm out}}, & \text{if } i_j \geq 0 \\ \frac{v_j}{v_{\rm out}}, & \text{otherwise} \end{cases} \end{aligned} \quad (12)$$

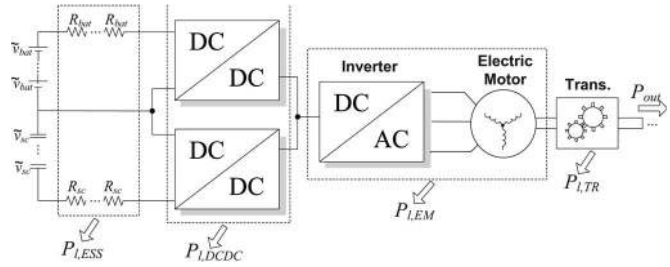

Fig. 4. Summary of the energy losses in the HESS and powertrain components.

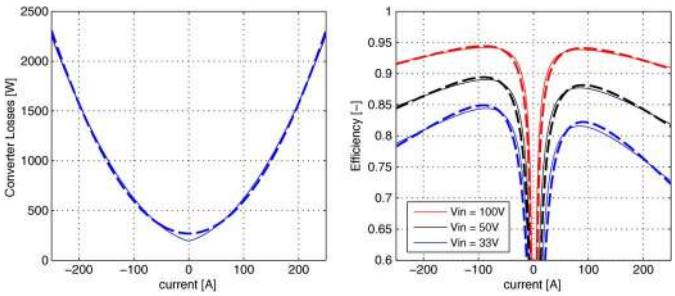

Fig. 5. Power losses and efficiency of the dc/dc converter ($C_0 = 191.9, C_1 = 1.69, C_2 = -0.1, C_3 = 0.026, C_4 = 0.001$, and $v_{\rm out} = 200$ V). The dashed line represents the quadratic approximation of the losses, obtained with (13).

where $v_{\rm out}$ is the converter output voltage, and C_m, $m = 0, \ldots, 4$, is the parameters of the loss model, which are dependent on the converter's components, e.g., equivalent series resistance of the inductor, the insulated-gate bipolar transistor, and the diode, energy dissipated in the turn on and off of the semiconductors, etc. (For a detailed account of the model derivation and its physical interpretation, see [31]). Fig. 5 shows the power losses of the dc/dc converter under consideration for the uCar vehicle, which is based on the SKM 600GB066D power semiconductor and an inductor with approximately 25 mΩ of equivalent series resistance. From these results, it is interesting to point out that, although the efficiency of the converter is dependent on the input voltage, the absolute value of the power losses appears to be little affected by the input voltage. Furthermore, one can also verify that, for this particular converter, the power losses seem to be dominated by the quadratic term of (12). Motivated by these observations, and to facilitate the incorporation of the converter losses in the (optimal) sizing problem, $P_{l,\,\rm DCDC}(t)$ will be approximated with the following quadratic model:

$$P_{l,\,\rm DCDC}(t) \approx \sum_{j \in \{\rm bat,\,sc\}} D_0 + D_1 i_j^2(t). \tag{13}$$

As shown in Fig. 5 (dashed lines), the errors introduced by this approximation are negligible.

After increasing the source's voltage to the levels required by the dc bus, the next stage is to generate the torque/force necessary for the EV motion. As shown in Fig. 4, this torque is produced through the electrical motor and its value adjusted by the dc/ac power converter (also known as the inverter). Although the energy losses of these components can be analytically determined (see, e.g., [34] and [35]), this paper follows a more pragmatic approach, based on efficiency maps. Accordingly, we will fit the efficiency map of the motor plus inverter, provided by the manufacturer or extracted from experimental tests, using the following approximation function:

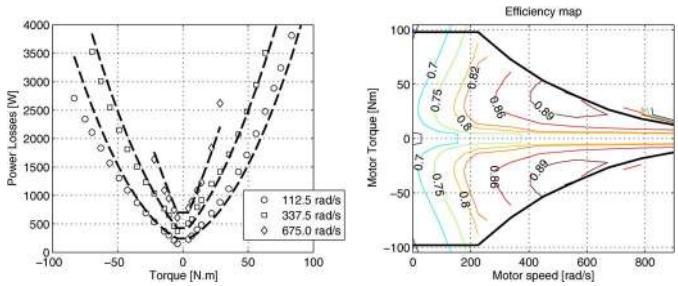

Fig. 6. Power losses and efficiency of the electric motor plus inverter, which is based on a 25-kW permanent-magnet motor retrieved from the QSS library [36]. The dashed line in the left plot represents the losses approximation obtained with (14).

$$P_{l,\,\rm EM}(t) = \mathbf{M}^T \varphi\left(T(t),\, \omega(t)\right) \tag{14a}$$

$$\varphi(T,\, \omega) = \left[\, 1 \quad |\omega| \quad |T| \quad |T\omega| \quad T^2 \quad \omega^2 \,\right] \tag{14b}$$

$$\omega(t) = \frac{G}{r} V(t) \quad T(t) = \frac{P_{\rm out}(t) + P_{l,\,\rm TR}(t)}{\omega(t)} \tag{14c}$$

where T is the motor torque, ω is the motor speed, G is the reduction ratio between the motor and the wheel, r is the wheel radius, and $\mathbf{M} \in \mathbb{R}^6$ is the parameter of the loss model. Similar to the dc/dc converter, the majority of the parameters in $\mathbf{M}$ have physical meaning, e.g., M_5 is associated with the copper losses, M_2 with hysteresis losses, and M_6 with eddy current losses [34]. Fig. 6 shows the efficiency map and power losses for the motor plus inverter considered for the vehicle, as well as the power losses resulting from the approximation (14). Despite the existence of some fitting errors, these are relatively low and still acceptable for sizing purposes.

The final element in the vehicle powertrain is the transmission, which, from a practical perspective, can be modeled as a constant efficiency component, i.e., [30]

$$P_{l,\,\rm TR}(t) \approx |P_{\rm out}(t)|\,(1 - \eta_{\rm TR}) \tag{15}$$

where $\eta_{\rm TR}$ is the transmission efficiency.

III. Filter-Based Sizing

After establishing the simplified source's models, the first methodology for the HESS sizing will now be described. As mentioned in Section I, the sizing process is dependent on the energy management strategy employed to split the power among the sources. There are many possibilities for performing this division, ranging from optimal approaches [9], [10], machine learning [11], and simple heuristics, such as the filter-based allocation [12], [37], [38]. Here, the sizing of the HESS will be performed supposing that the power blending among the sources is based on low/high-pass filters. The filter-based allocation policy is normally motivated by the complementary features presented by each source. For instance, SCs generally have high peak power capability and low energy, whereas batteries display opposite features (higher energy storage

capability and moderate peak power). These intrinsic features cause the SCs to be regarded as an auxiliary source that should provide the power peaks during the acceleration/braking transients, which can be seen as the high-frequency content of $P_{\rm out}$, whereas the batteries are responsible for ensuring the steady-state power delivery, associated with the low-frequency content of $P_{\rm out}$. It is based on this line of reasoning that the frequency-based power allocation emerges as one of the most simple and appealing strategies for the real-time managing of HESS's [12], [37], [38], and which motivated us to use it in the first sizing approach. Based on this allocation policy, our goal here is to find the number of batteries $(n_{\rm bat})$ and SCs $(n_{\rm sc})$ that minimize the cells' acquisition costs, satisfying both the power and energy required by the nominal driving cycle.

A. Problem Formulation

As a starting point, consider the decomposition of the power requested to the HESS as a sum of low-frequency and high-frequency signals, i.e.,

$$P_{\rm out}(t) = \mathcal{L}_\tau\left\{P_{\rm out}(t)\right\} + \mathcal{H}_\tau\left\{P_{\rm out}(t)\right\} \tag{16}$$

where $\mathcal{L}_\tau$ and $\mathcal{H}_\tau$ are the first-order low-pass and high-pass operators, respectively, with time constant equal to τ (in seconds), and are defined as

$$\mathcal{L}_\tau\left\{x(t)\right\} = \left\{y(t) \mid \tau\dot{y}(t) + y(t) = x(t)\right\} \tag{17a}$$
$$\mathcal{H}_\tau\left\{x(t)\right\} = x(t) - \mathcal{L}_\tau\left\{x(t)\right\}. \tag{17b}$$

By exploring the linear property of these operators, and taking into account (7), the power decomposition can be further expanded as

$$\begin{aligned}\mathcal{L}_\tau\{P_{\rm out}\} &= \mathcal{L}_\tau\left\{P_0(t)\right\} + \mathcal{L}_\tau\left\{\Delta_P(t)\right\}(n_{\rm bat}m_{\rm bat} + n_{\rm sc}m_{\rm sc}) \\ &= P_0^{\mathcal{L}}(t) + \Delta_P^{\mathcal{L}}(t)(n_{\rm bat}m_{\rm bat} + n_{\rm sc}m_{\rm sc})\end{aligned} \tag{18}$$

where $P_0^{\mathcal{L}}$, and $\Delta_P^{\mathcal{L}}$ are the low-pass components of P_0 and Δ_P. Likewise, $\mathcal{H}_\tau\{P_{\rm out}(t)\}$ can be represented using the "high-pass" components $P_0^{\mathcal{H}}$ and $\Delta_P^{\mathcal{H}}$, omitted here for brevity. Regarding the energy of the driving cycle, a similar decomposition can be established, i.e.,

$$\begin{aligned}E_{\rm out}(t) &= \int_0^t \left(P_0^{\mathcal{L}}(s) + \Delta_P^{\mathcal{L}}(s)(n_{\rm bat}m_{\rm bat} + n_{\rm sc}m_{\rm sc})\right) ds \\ &\quad + \int_0^t \left(P_0^{\mathcal{H}}(s) + \Delta_P^{\mathcal{H}}(s)(n_{\rm bat}m_{\rm bat} + n_{\rm sc}m_{\rm sc})\right) ds \\ &= E_0^{\mathcal{L}}(t) + \Delta_E^{\mathcal{L}}(t)(n_{\rm bat}m_{\rm bat} + n_{\rm sc}m_{\rm sc}) + E_0^{\mathcal{H}}(t) \\ &\quad + \Delta_E^{\mathcal{H}}(t)(n_{\rm bat}m_{\rm bat} + n_{\rm sc}m_{\rm sc})\end{aligned} \tag{19}$$

where $E_0^{\mathcal{L}}$, $E_0^{\mathcal{H}}$, and $\Delta_E^{\mathcal{L}}$, $\Delta_E^{\mathcal{H}}$ are the low-pass and high-pass components of the driving cycle's energy E_0 and energy increments Δ_E.

Now, suppose that: 1) the maximum energy provided by each cell e_j (in wattseconds per cell), as well as its peak power capability p_j (in watts per cell), are known; and 2) the energy losses of the powertrain components, presented in Section II-C, can be lumped together, and approximated as a single equivalent component with constant efficiency $\hat{\eta}_{\rm PT}$.

Remark 1: It is important to mention that the aforementioned approximations normally carry with them nonnegligible modeling errors. For example, in practice, it is well known that the power capability of the SCs is strongly dependent on its SOC and that the powertrain's energy efficiency depends on the vehicle's operating point, which varies in time. Despite these strong assumptions, our interest here is just to develop a simple tool that allows the designer to gain quick insight on the fundamental issues and tradeoffs related to the sizing of HESS.

Spurred by the frequency-based power allocation, we will constrain the admissible number of cells of batteries and SCs to the following set:

$$\begin{aligned}\Phi(\tau) = \{(n_{\rm bat}, n_{\rm sc}) : &p_{\rm bat}n_{\rm bat}\hat{\eta}_{\rm PT} \\ &\geq P_0^{\mathcal{L}}[k] + \Delta_P^{\mathcal{L}}[k](n_{\rm bat}m_{\rm bat} + n_{\rm sc}m_{\rm sc})p_{\rm sc}n_{\rm sc}\hat{\eta}_{\rm PT} \\ &\geq P_0^{\mathcal{H}}[k] + \Delta_P^{\mathcal{H}}[k](n_{\rm bat}m_{\rm bat} + n_{\rm sc}m_{\rm sc})e_{\rm bat}n_{\rm bat}\hat{\eta}_{\rm PT} \\ &\geq E_0^{\mathcal{L}}[k] + \Delta_E^{\mathcal{L}}[k](n_{\rm bat}m_{\rm bat} + n_{\rm sc}m_{\rm sc})e_{\rm sc}n_{\rm sc}\hat{\eta}_{\rm PT} \\ &\geq E_0^{\mathcal{H}}[k] + \Delta_E^{\mathcal{H}}[k](n_{\rm bat}m_{\rm bat} + n_{\rm sc}m_{\rm sc}) \\ &k = 0, \ldots, N, \quad 0 \leq n_{\rm bat} \leq \overline{n}_{\rm bat}, \quad 0 \leq n_{\rm sc} \leq \overline{n}_{\rm sc}\}\end{aligned}$$

where $\bullet[k] = \bullet(kT_s)$, T_s is the sampling time, N is the number of points employed in the driving cycle discretization, and $\overline{n}_{\rm bat}$, $\overline{n}_{\rm sc}$ is the maximum number of cells. Inspecting the formulation of this set, one can find that the first two linear inequalities specify that the battery (SC) should provide the low (high) frequency content of the driving cycle, whereas the third and fourth inequalities are concerned with similar arguments but are applied to the energy requirements. The time constant τ employed in the frequency splitting also plays an important role in the construction of the $\Phi(\tau)$, and to some extent, it can be seen as a parameter that controls the degree of hybridization in the ESS [see Fig. 7(a)]. In fact, it is interesting to note that, as limit cases, we have ESS's where only batteries $(\tau = 0)$ or SCs $(\tau = \infty)$ are employed. Furthermore, the power and energy constraints of Φ should be, in theory, evaluated for all the time instants of the driving cycle. However, from a practical point of view, it is expected that the set Φ will be dominated by the power and/or energy peaks required by the EV. Consequently, to quickly approximate Φ, we can replace $P_0^{\mathcal{L}}[k]$, $\Delta_P^{\mathcal{L}}[k]$, $P_0^{\mathcal{H}}[k]$, $\Delta_P^{\mathcal{H}}[k]$, $E_0^{\mathcal{L}}[k]$, $\Delta_E^{\mathcal{L}}[k]$, $E_0^{\mathcal{H}}[k]$, and$\Delta_E^{\mathcal{H}}[k]$ by their upper bounds (e.g., $\overline{P_0^{\mathcal{L}}} = \max_k P_0^{\mathcal{L}}[k]$), which enables us to reduce the number of inequalities to only four. Usually, we found that this simplification generally introduces negligible errors [see, e.g., the blue constraints in Fig. 7(b)].

Based on this setting, it is our intention to find the triplet $(n_{\rm bat},\, n_{\rm sc},\, \tau) \in \Phi(\tau) \times [\underline{\tau},\, \overline{\tau}]$ that minimizes the cells' cost, which can be posed as

$$\begin{aligned}\min_{n_{\rm bat}, n_{\rm sc}, \tau} \quad & c_{\rm bat}n_{\rm bat} + c_{\rm sc}n_{\rm sc} \\ \text{s.t.} \quad & \boldsymbol{A}(\tau)\begin{bmatrix} n_{\rm bat} \\ n_{\rm sc}\end{bmatrix} \leq \boldsymbol{B}(\tau) \\ & \underline{\tau} \leq \tau \leq \overline{\tau}\end{aligned} \tag{20}$$

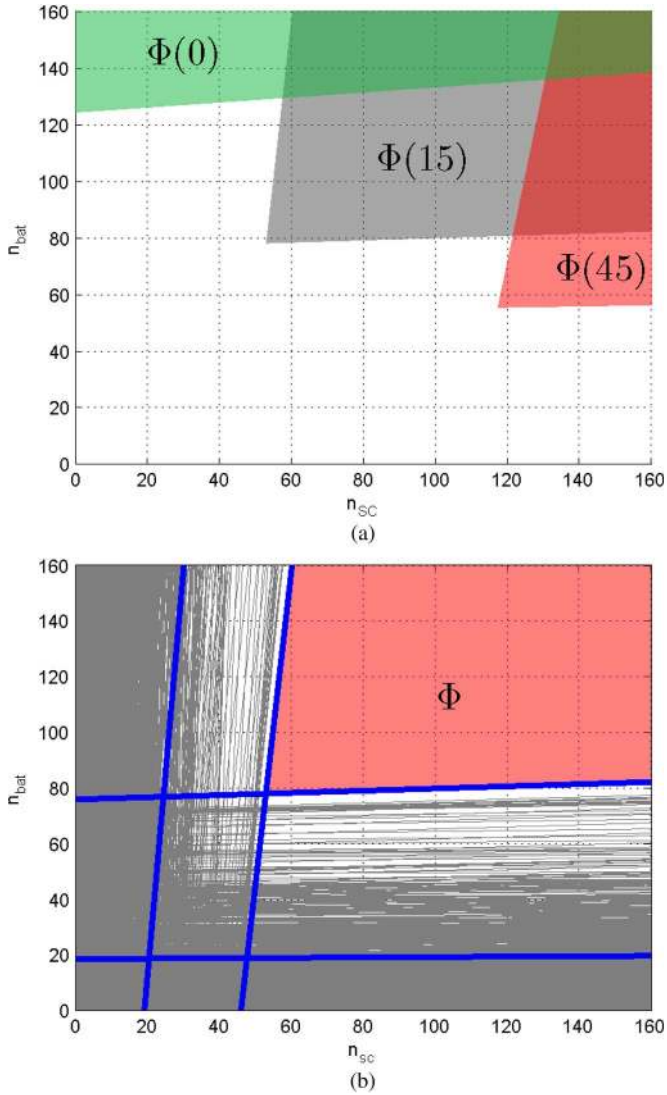

Fig. 7. (a) Typical example of the domain $\Phi(\tau)$. (b) Inequality constraints employed in the construction of $\Phi(\tau)$ set during the ARTEMIS road driving cycle. (Gray lines represent the power and energy inequalities for all the points in the driving cycle; the dominant inequalities are shown in blue).

where $\boldsymbol{A} \in \mathbb{R}^{p\times 2}$ and $\boldsymbol{B} \in \mathbb{R}^{p\times 1}$ represent the matrix notations of the p inequalities that can be extracted from (20). This problem depends on τ in a nonlinear way, which may pose some challenges to the numerical solver. To attenuate this issue, we will solve the optimization problem in a two-step process. First, notice that, for a fixed τ, both the constraints and cost function are linear in $(n_{\mathrm{bat}}, n_{\mathrm{sc}})$; therefore, (20), as long as τ is constant, can be treated as a linear programming problem. Based on this observation, we can straightforwardly evaluate (20) for a possible list of admissible time constants $[\tau_1, \ldots, \tau_M]$, generating a family of sizing results and cost function, parameterized in τ, i.e., $J_A(\tau)$, $n_{\mathrm{bat}}(\tau)$, $n_{\mathrm{sc}}(\tau)$. The optimal solution can be then readily extracted by selecting the $J_A(\tau)$ with minimum cost, which represents the second and final steps in the solving process. In the numerical optimization literature, this approach is also known as the "optimizing over some variables" technique [39, Ch. 4].

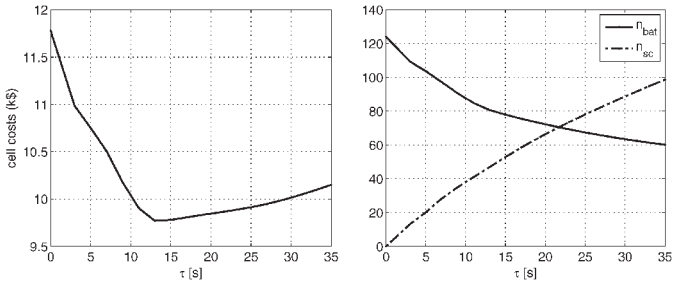

Fig. 8. $J_A(\tau)$, $n_{\mathrm{bat}}(\tau)$, $n_{\mathrm{sc}}(\tau)$ when sizing the HESS to satisfy the ARTEMIS road cycle.

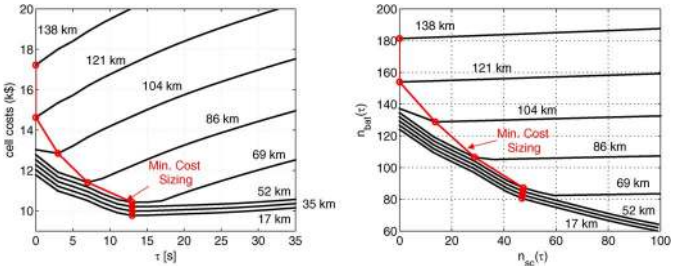

Fig. 9. Evaluation of $J_A(\tau), n_{\mathrm{bat}}(\tau), n_{\mathrm{sc}}(\tau)$ for the ARTEMIS road driving cycle (repeated several times to increase the range requirements).

B. Sizing Example and Discussion

With the purpose of preliminarily evaluating the filter-based sizing, we will now apply this methodology to build a battery–SC ESS capable of meeting the requirements of the ARTEMIS road cycle (the parametric details of the EV and energy sources are described in Table I). Fig. 8 shows the intermediate results associated with the first step in the resolution of (20), i.e., $J_A(\tau)$, $n_{\mathrm{bat}}(\tau)$, $n_{\mathrm{sc}}(\tau)$. These results confirm that the parameter τ indirectly controls the degree of hybridization of the ESS: 1) for $\tau \approx 0$, we have the case where only batteries are employed, showing a relatively high installation cost (11.8 k$); 2) as we increase τ, it is apparent that the cost decreases, reaching a minimum at $\tau = 13$ s (9.8 k$); and 3) ultimately, for $\tau > 13$ s, the usage of SCs becomes more relevant, which again raises the costs. A second sizing example is shown in Fig. 9, for the case where the driving cycle's range increases progressively up to 138 km. Looking at the J_A evolution, it is worth noting that, for EV ranges between 17 and 69 km, the degree of hybridization remains almost constant, having minimum cost for $\tau = 13$ s. On the other hand, when the range requirements exceed 69 km, the SCs' use becomes less beneficial (from an installation cost point of view), and the degree of hybridization, as well as the number of SCs, is reduced. This behavior suggests that there is a range threshold where the hybridization of battery–SCs provides the maximum gains (in this example, the threshold is 69 km).

In conclusion, the filter-based sizing presented here is a simple numerically efficient tool, offering a rapid way to determine an order of magnitude estimate for $(n_{\mathrm{bat}}, n_{\mathrm{sc}})$. Further, by playing with the τ parameter, we can also gain valuable insight on the tradeoffs associated with the SCs' inclusion in the HESS. However, due to some simplifications (see Remark 1), this approach only provides a rough approximation of the ideal

sizing. Perhaps, the most notorious drawback is the assumption of constant peak power and energy-per-cell metrics (e_j and p_j). In practice, it is well known that these metrics are hardly constant and depend on the source's SOC and the load power being requested. Given that these factors were, so far, neglected, conservative estimates of e_j and p_j have to be applied, which, as we will see later, generally limit the performance of the filter-based sizing.

IV. Optimal Sizing

To overcome the limitations of the filter-based sizing, a second sizing methodology, based entirely on an optimization framework, will now be developed. As already discussed, the sizing process is intrinsically connected to the strategy employed in the energy management of the sources. From a theoretical standpoint, the energy management is, in its essence, an optimal control problem, i.e., the goal is to find a power division between the sources that minimize a given performance criterion (e.g., energy losses [10] or the battery stress [9]). Similarly, the sizing process can also be posed as an optimization problem, targeting, for example, the minimization of the source's installation costs. Consequently, since both the sizing and the energy management are naturally formulated within an optimization setting, it is convenient to consider both tasks simultaneously. In other words, the main idea here is to combine the HESS sizing with the (optimal) energy management algorithm.

A. Problem Formulation

As a performance index, our goal is to minimize a weighted version of the total cost of ownership of the EV, including the cells' acquisition costs ($c_{\rm bat}n_{\rm bat} + c_{\rm sc}n_{\rm sc}$) and the charging cost of the EV during its expected lifetime. This latter cost is defined as

$$\begin{aligned} J_R &= \gamma \int_0^{T_{\rm dc}} \left(P_{\rm out}(t) + P_l(t)\right) dt \\ &\approx \gamma T_s \sum_{k=0}^{N-1} \left(P_{\rm out}[k] + P_l[k]\right) \end{aligned} \tag{21}$$

with N being the number of points employed in the driving cycle discretization and γ (in \$/Ws) being a constant parameter that translates the vehicle's energy consumption to an economic cost. One possible way to define the parameter γ is to consider

$$\gamma = \sum_{y=1}^{N_y} l_y \alpha_y \tag{22}$$

where N_y is the estimated lifetime of the HESS (in years), l_y is the number of journeys that the vehicle is expected to perform in the year $y \in [1, 2, \ldots, N_y]$, and α_y is the cost (\$/Ws) of the electricity in the year y. Naturally, l_y and N_y should be selected having in mind the limitation of charge/discharge cycles of the HESS.

The combined sizing/energy management problem is defined as

$$\begin{aligned} \min \quad & \left(w \sum_{j\in\{\rm bat,\,sc\}} c_j n_j\right) + \gamma T_s \sum_{k=0}^{N-1} \left(P_{\rm out}[k] + P_l[k]\right) \\ \text{s.t.} \quad & q_j[k+1] = q_j[k] - i_j[k]\frac{T_s}{\overline{Q}_j}, \quad q_j[0] = q_{j,0} \\ & \tilde{v}_j[k] = a_j + b_j q_j[k] \\ & \sum_{j\in\{\rm bat,\,sc\}} n_j \tilde{v}_j[k] i_j[k] = P_{\rm out}[k] + P_l[k] \\ & P_0[k] + \Delta_P[k] \sum_{j\in\{\rm bat,\,sc\}} n_j m_j = P_{\rm out}[k] \\ & \mathbf{M}^T \varphi\left(T[k], \omega[k]\right) + |P_{\rm out}[k]|\left(1 - \eta_{\rm TR}\right) \\ & + \sum_{j\in\{\rm bat,\,sc\}} D_0 + \left(D_1 + n_j R_j\right)\left(i_j[k]\right)^2 = P_l[k] \\ & T[k] = \frac{P_{\rm out}[k] + |P_{\rm out}[k]|\left(1 - \eta_{\rm TR}\right)}{\omega[k]} \\ & \underline{q_j} \le q_j[k] \le \overline{q_j}, \quad 0 \le n_j \le \overline{n}_j \\ & \underline{i_j} \le i_j[k] \le \overline{i_j}, \quad \frac{1}{N+1}\sum_{k=0}^{N} i_j[k]^2 \le \chi_j^2 \overline{I}_{rms,j}^2 \\ & k \in \{0, \ldots N\}, \quad j \in \{\text{bat, sc}\} \end{aligned} \tag{23}$$

where $q_{j,0}$ is the initial SOC, $\underline{q_j}/\overline{q_j}$ is the minimum/maximum allowable SOC, $\underline{i_j}/\overline{i_j}$ is the minimum/maximum peak currents of each source, and $\overline{I}_{{\rm rms},\,j}$ is the maximum RMS current. By examining the problem constraints, one can readily verify that the first two are the result of the discretization (with the Euler method) of the battery/SC cells' model, defined in (1). The third, fourth, and fifth impose the balance between the power delivered by the HESS, the powertrain losses, and the vehicle load. The sixth establishes the operating point of the electric motor, which is important to calculate its losses, whereas the last set of constraints is related to the SOC and current limits. The problem also contains parameter $\chi_j \in [0,\,1]$ that can be explored by the designer to reduce the RMS current in the cells. This is particularly useful to limit the stress in the battery pack. As for the cost function, it is worth highlighting the presence of the tradeoff factor $w \in [0,\,1]$, which enables the designer to pursue different goals, such as the following:

- $w = 1$, which aims to minimize the total cost of the vehicle (cells' cost plus running costs);
- $w = 0$, which focuses only on the minimization of the vehicle's running costs $= \gamma E_{\rm in}$, which are directly related to the vehicle's energy consumption $E_{\rm in}$;
- $w \in (0,\,1)$ constitutes a tradeoff between the cells' cost and the energy consumption of the EV.

To a certain extent, it is expected that the two goals under consideration, cells' cost and energy efficiency, will conflict with each other. For example, if the aim is to build an EV with low energy consumption ($w = 0$), then it is predictable that the number of SCs, i.e., the most energy efficient and lighter source,

will be higher, which may lead to a significant increase in the cells' cost. Conversely, if the total cost of the HESS is the main concern $(w = 1)$, it is expected that the number of batteries and SCs will be reduced, which, in principle, will increase the energy losses, particularly Joule losses. In this context, it is the designer's responsibility to decide, through the parameter w, an appropriate tradeoff between cost and energy efficiency that best suits the requirements for the HESS.

Remark 2: Fixing, *a priori*, the number of cells $n_{\rm bat}, n_{\rm sc}$ in (23) produces the typical "benchmark" problem for the optimal power allocation between multiple sources.

B. Solving Methodology

To handle the optimization problem (23) we start by translating it to the A Mathematical Programming Language language [40], an environment dedicated to modeling large-scale optimization problems. The main advantages in using this environment are as follows: 1) The formulation is carried out in an almost natural language, making it very easy to specify and modify the decision variables, constraints and all the other elements in the problem; 2) it allows the user to interface with different types of numerical solvers (linear, nonlinear, open source, commercial, etc.); and 3) it automatically generates the gradient information for the problem, based on automatic differentiation strategies [41], which is critical for the convergence of the numerical optimization methods. After the problem's translation, we employed the IPOPT solver, an open-source nonlinear programming solver, to numerically extract the solution for the problem (see [42] for a detailed account of the inner details of the algorithm).

In addition to the numerical solver and the gradient information, the initial guess for the decision variables represent another key aspect of the algorithm performance. To cope with this challenge, we start by determining an initial estimative for the number of cells $(\hat{n}_{\rm bat}, \hat{n}_{\rm sc})$, using the output of the filter-based sizing, discussed earlier. The value of the remaining decision variables are then estimated by solving the "benchmark" power allocation, mentioned in Remark 2, i.e., (23) is relaxed by fixing the number of cells $(\hat{n}_{\rm bat}, \hat{n}_{\rm sc})$. As will be shown later, we found this initialization procedure to be very effective and able to successfully handle longer driving cycles $(N > 8000)$.

At this stage, it is worth discussing some of the shortcomings of the optimization-based sizing adopted in this paper. First, notice that, while the cost function and the majority of the constraints are linear, the power balance constraints have equalities involving the product of decision variables (e.g., $n_j \tilde{v}_j[k] i_j[k]$), as well as quadratic terms in the current, which makes the problem nonconvex (recall that a convex problem only accepts affine equalities [39]). Thus, the resulting optimization problem is nonlinear and nonconvex, which poses some numerical challenges to obtain global optimal solutions. Nevertheless, we will show later that these (locally optimal) solutions still perform better than the solutions obtained with the simplified filter-based sizing.

Second, the sizing process is performed under the assumption of an ideal energy management, with advance access to the driving cycle profile. Since this information will hardly be available during the real-time operation, the sizing solutions may be slightly optimistic. In any case, the optimal sizing is still of practical interest, as it allows us to obtain a benchmark solution, establishing the maximum gains that can be achieved with the ESS hybridization.

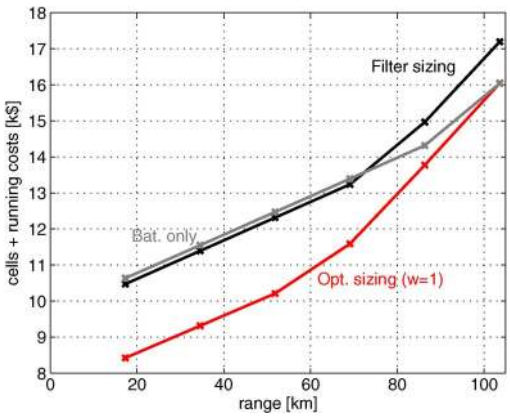

Fig. 10. Combined costs (cells plus energy charge of the EV) for different ESSs: 1) battery only; 2) HESS, sized with the filter; and 3) HESS, sized with the optimal approach $(w = 1)$. The ARTEMIS road was used as the nominal driving cycle.

Third, the problem formulation also assumes that the numbers of cells, $n_{\rm bat}$, $n_{\rm sc}$, are real numbers, whereas in practice, it must belong to an integer range. This approximation brings important advantages to the numerical solution of the problem since it allows us to avoid the use of more complicated mixed-integer nonlinear programming solvers. In addition, as the HESS is normally composed of a large number of batteries and SCs, it is expected that the rounding errors in $n_{\rm bat}$, $n_{\rm sc}$ will have a minor impact in the final solution [19].

V. Case Study Example

The two sizing methodologies described earlier will be applied here to design the HESS of a future version of the uCar vehicle (see Table I for the parametric details). The ARTEMIS road cycle [43] will be used as the basic speed profile that the EV should meet, which means a top speed of 111 km/h, maximum accelerations up to 8.5 km/h/s^2, and a minimum range of 17.23 km, as illustrated in Fig. 3. To investigate different demands in terms of the EV autonomy, the ARTEMIS road cycle was repeated several times (up to eight times). For comparison purposes, we also evaluated the case where the battery is used as the single source of the EV [i.e., fixing $n_{\rm sc} = 0$ in (23)], which is referred to as the "battery only" solution hereafter.

A. Minimization of Vehicle's Total Costs

1) Filter-Based Sizing versus Optimal Sizing: Figs. 10 and 11 show the sizing results for the situations with: 1) battery only; 2) filter-based sizing; and 3) optimal sizing, targeting the minimization of the vehicle's total cost $(w = 1)$. Broadly speaking, the filter-based solution displays a similar trend to that of the optimal sizing, i.e., as the range increases, the number of SCs is reduced and the batteries increase. However, due to the conservative estimates of e_j, p_j, and $\hat{\eta}_{\rm PT}$ discussed

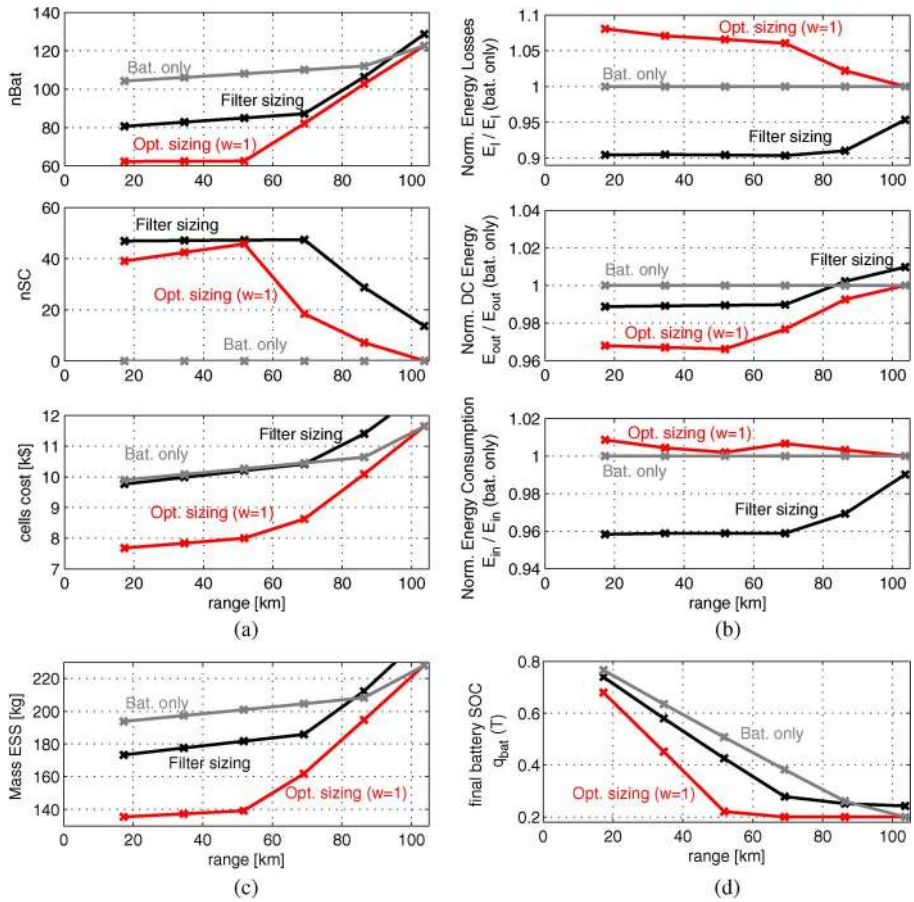

Fig. 11. Performance comparison between different ESS: 1) battery only; 2) HESS, sized with the filter; and 3) HESS, sized with the optimal approach ($w = 1$). The ARTEMIS road was used as the nominal driving cycle. (a) Sizing results. (b) Energy metrics, ($E_{\rm in} = E_{\rm out} + E_l$)

in Section III-B, the filter-based solution normally generates an oversized HESS, requiring a greater number of cells and installation costs. Regarding the energy losses shown in Fig. 11(b), it is interesting to note that, in comparison with the "battery only" solution, the HESS, sized with the optimal approach, shows a slight increase in the powertrain losses (E_l). At first glance, one might expect that the "battery only" solution would be a less efficient storage system, given that no auxiliary aid is provided by the SCs. Nonetheless, the fact remains that, as this ESS configuration entails a larger number of battery cells (105–120, depending on the range), the Joule losses tend to be reduced. This larger number of battery cells also raises the input voltage of the dc/dc converter, which contributes to higher operation efficiency for this component (see Fig. 5). Notice that, at this stage, our goal is centered on the minimization of the cells and running costs of the EV ($w = 1.0$), and not on the vehicle's energy efficiency (which will be discussed later on).

Finally, these results also reveal that the filter-based sizing is the solution with minimum energy consumption and losses (as a result of being oversized).

2) Detailed Analysis of the Optimal Sizing ($w = 1.0$): Since the optimal sizing provides better overall performance (see Fig. 10), we will now discuss in more detail the results obtained with this method. Referring again to Fig. 11(a), it can be verified that, if the desired range per charge of the EV is below 50 km, the inclusion of the SC in the HESS, i.e., sized with the optimal approach, contributes to a significant downsize of the battery pack (from ∼105 cells to only ∼63 cells). This downsize has positive and negative consequences. On the plus side, we can see that the cost of the cells is significantly reduced: using a single battery pack to meet the 50-km range needs an investment of ∼10.3 k$, while the HESS only requires ∼8 k$. This represents a 22.2% reduction in the cells' costs. Another advantage of the battery downsize is the decrease in the ESS storage mass [see Fig. 11(c)], which then contributes to a reduction of 3% in the energy required by the driving cycle $E_{\rm in}$, as shown in Fig. 11(b). The main inconvenience associated with the battery downsize is the increase in the energy losses E_l, the causes of which were already discussed. Nonetheless, these higher energy losses are compensated for by the energy savings resulting from the lighter ESS, and in the end, the overall energy consumption of the vehicle $E_{\rm in}$ is little affected; as shown in Fig. 11(b), for the HESS sized with the optimal approach, $E_{\rm in}$ exhibits a small increase in the range of 0.2%-0.9%.

On the other hand, when the EV range requirements increase above 50 km, there is a decline in the number of SC cells, and the HESS sizing ends up converging to the situation where only batteries are employed. To explain this trend, it is helpful to look at the final SOC value of the battery ($q_{\rm bat}(T_{\rm dc})$), shown in Fig. 11(d). From these results, it can be concluded that, for driving ranges inferior to 50 km, the battery is not completely discharged at the end of the driving cycle, which suggests that the (peak) power constraint is the dominant factor in the ESS sizing. Thus, given the high power capability of the SCs, there

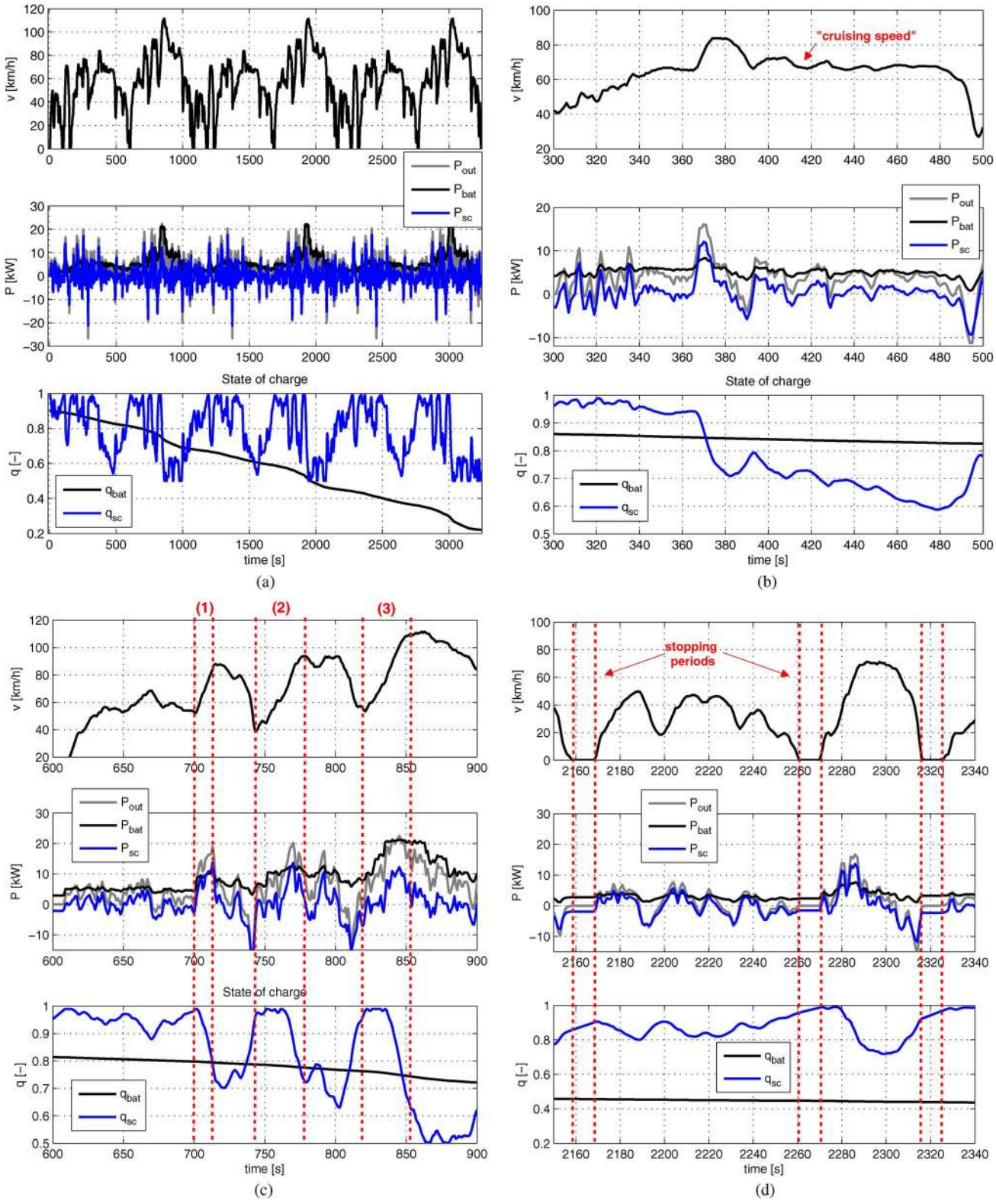

Fig. 12. Energy management results for the optimal approach ($w = 1.0$); the range requirement for this simulation was set at 52 km, and the ARTEMIS road was used as the nominal driving cycle. (a) Full driving cycle. (b) "Cruising speed." (c) Strong acceleration periods. (d) Stopping periods.

is more freedom to reduce the battery power stress, which results in its downsize. However, as the EV autonomy increases above 50 km, the energy constraint becomes more relevant (notice that $q_{\mathrm{bat}}(T_{\mathrm{dc}})$ is close to the minimum limit), and the sizing is dominated by the energy demand. Since the SCs have very low energy densities, the benefit of this source, from an installation cost perspective, diminishes as the range demand increases. As a side note, it is worth mentioning that this trend was also predicted by the filter-based sizing, exemplified in Fig. 9.

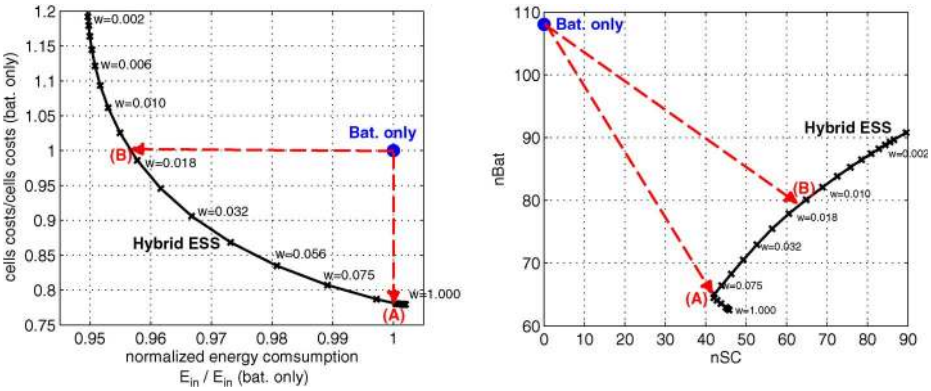

Fig. 13. Tradeoff between cell cost and energy efficiency, when sizing the HESS with the optimal approach. The ARTEMIS road (50 km) was used as the nominal driving cycle.

3) Energy Management With Nominal Driving Cycle: In addition to the sizing task, the optimal approach also enables us to determine the ideal power split between the batteries and SCs. For example, Fig. 12 shows the power sharing between the sources, obtained when using (23) to size the storage unit for a range of 50 km ($n_{\rm bat} = 63$, $n_{\rm sc} = 46$). Analyzing these results, one can find that, when the vehicle is traveling at "cruising" speed, the battery should provide (roughly) the low frequency content of the driving cycle power, whereas the SCs should respond to the high frequencies [see Fig. 12(b)]. This remark turns out to be very important for the development of causal allocation strategies: since the low/high frequency decomposition can be easily emulated through low/high-pass filters, the use of power allocation based on filters has become one of the most popular methods for the real-time managing of HESS [12], [37], [38].

Inspecting Fig. 12(c) reveals that, during acceleration and braking transients, the SC provides important assistance to the batteries. From a practical perspective, the main challenge in managing these transients is to decide when to deploy the limited charge of the SCs. For example, for transients with short duration, the SCs should be used as soon as the vehicle is accelerated [see, e.g., Fig. 12(c), zone 1]. On the other hand, for longer acceleration periods [see, e.g., Fig. 12(c), zones 2 and 3] the SC deployment should be reserved to the latter part of the transient, where its usage is more helpful to limit the peak power requested to the battery, as well as its losses. Predicting the duration of these acceleration transients, although easy for the noncausal setting proposed in (23), is extremely difficult for causal control systems and remains one of the ultimate challenges in the real-time energy management of HESS. Finally, one can also find that it is advantageous to keep charging the SCs during the period when the vehicle is stationary [see Fig. 12(d)].

B. Tradeoff Between Installation Cost and Energy Consumption

Up to now, the sizing of the HESS favored the economic factor by targeting the minimization of the total costs of ownership of the EV. However, the optimal sizing formulation contains a tuning parameter w that allows the designer to explore tradeoffs between cells' cost and energy efficiency. To illustrate how this tradeoff can be realized in practice, Fig. 13 shows the influence of w when sizing an HESS for a range of 50 km. Qualitatively, these plots show that, if we pretend to decrease the EV's energy consumption, then the number of cells (particularly the SCs) and the corresponding costs must be raised, which is in accordance with our engineer intuition. Additionally, in comparison with the "battery only" solution, the tradeoff curve of the HESS shows the following.

- using the same investment in cells as the "battery only" solution, the HESS reduces the energy consumption by 4% (see Fig. 13, point B);
- With the same energy consumption as the "battery only", the HESS can decrease the cells' costs by 22% (see Fig. 13, point A).

In conclusion, these results demonstrate that, with the optimal-based sizing, the designer has the option of selecting a tradeoff point that best suits the system requirements and the available budget for the EV construction.

1) Energy Management With Nonnominal Driving Cycles: Although the sizing task was carried out under the assumption of a nominal driving cycle, it is also worth investigating how the resulting HESS performs when the driving conditions deviate from nominal conditions. With this goal in mind, several numerical simulations were carried out for some typical driving cycles, such as the ECE15, ARTEMIS Urban, NYCC, FTP75, and SFTP S03 [43]. For each driving cycle, three types of ESS were considered: 1) battery only ($n_{\rm bat} = 109$, $n_{\rm sc} = 0$); 2) HESS ($n_{\rm bat} = 63$, $n_{\rm sc} = 46$), targeting the minimization of the vehicle's costs, $w = 1$; and 3) HESS ($n_{\rm bat} = 78$, $n_{\rm sc} = 61$), targeting a tradeoff between cost and energy efficiency, i.e., $w = 0.016$, which corresponds to point B in Fig. 13. In all the cases, the ESS was sized using (23) for a range of 50 km.

Fig. 14 shows the overall results of the various configurations under study. It can be seen that, in all the nonnominal driving cycles, the inclusion of the SCs reduces the energy consumption ($E_{\rm in}$) between 3% and 7.8%, being higher in the urban driving cycles (NYCC and ARTEMIS urban). To some extent, these results were expected since, in urban scenarios, with short distances and where the start/stop patterns are frequent, it is reasonable to expect that the aid provided by the SC will be more beneficial to the energy consumption of the EV.

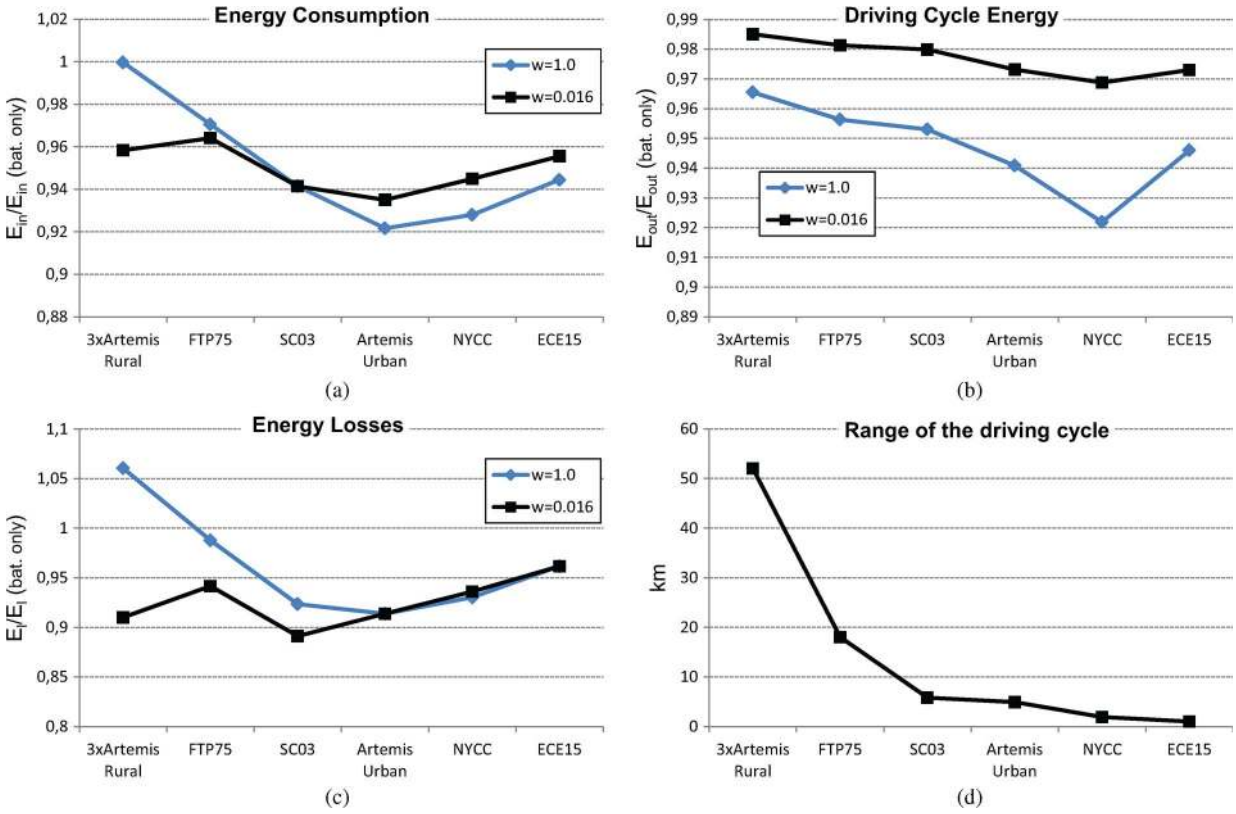

Fig. 14. Normalized energy consumption metrics of the HESS, when subject to nominal (ARTEMIS Rural, 50 km) and nonnominal driving cycles.

Another factor that deserves to be highlighted is the influence of parameter w. It was already verified that, when sizing the HESS with minimum cost $(w = 1)$, the energy savings in E_{in} throughout the nominal driving cycle are almost null. However, this property cannot be generalized to nonnominal driving cycles, as shown in Fig. 14. By the same token, the HESS sized with $w = 0.016$, although providing 4% energy savings in the nominal driving cycle, evidences higher energy consumption (in comparison with $w = 1$) for the urban driving cycles. The reason for this apparent contradiction is related to the interplay that exists between energy losses E_l, the driving cycle's energy E_{out}, and the duration of the driving cycle, which is shown in Fig. 14. In particular, the lighter HESS $(w = 1)$ seems to pay off in urban scenarios (despite the higher energy losses), whereas the more energy efficient,[1] HESS $(w = 0.016)$ is penalized by the heavier cells' mass; the opposite behavior is verified when the cycle's range increases (see, e.g., the consumption for the FPT75 case).

VI. Conclusion

In this paper, two methodologies for the sizing of HESS composed of batteries and SCs have been developed. The main attractiveness of these methods resides in the combination of the energy management problem together with the sizing task. The first method, called filter-based sizing, employs a simple frequency power decomposition to manage the HESS and assumes that the peak power and energy capabilities of each source are known. This approach, formulated as a linear programming problem, is numerically efficient, and it provides insight into the basic mechanisms associated with battery–SC hybridization. However, due to the approximations and simplifications adopted in the formulation, it is only able to provide a rough estimate of the ideal sizing. To increase the accuracy of the sizing process, a full optimization-based approach, i.e., for both energy management and sizing problems, was then proposed. This second method allows us to incorporate more accurate energy loss models of the powertrain components in the sizing task and also enables pursuing the tradeoffs between installation costs and energy efficiency. For the particular parametric configuration under study and assuming that the daily ranges inferior to 50 km, it was concluded that, by adding SCs to the ESS, the overall costs (installation plus charging) of the EV can be reduced by almost 20%. In addition, depending on the type of driving cycle, the HESS showed energy savings of up to 7.8%, representing an important contribution toward an increase in the vehicle's range.

As future work, it is our intention to incorporate additional performance metrics in the sizing problem, such as the battery stress and degradation. Further, we also plan to tackle the real-time energy management problem, i.e., the design of a power split strategy for the HESS without having prior knowledge of the vehicle's speed profile.

[1] In the sense that the energy losses are minimial.

References

[1] L. Guzzella and A. Sciarretta, *Vehicle Propulsion Systems: Introduction to Modeling and Optimization*. Berlin, Germany: Springer-Verlag, 2007.

[2] S. Vazquez, S. M. Lukic, E. Galvan, L. G. Franquelo, and J. M. Carrasco, "Energy storage systems for transport and grid applications," *IEEE Trans. Ind. Electron.*, vol. 57, no. 12, pp. 3881–3895, Dec. 2010.

[3] A. Dinger, R. Martin, X. Mosquet, M. Rabl, D. Rizoulis, M. Russo, and G. Sticher, "Batteries for electric cars: Challenges, opportunities, and the outlook to 2020," Boston Consulting Group, Boston, MA, USA, 2010.
[4] A. Khaligh and Z. Li, "Battery, ultracapacitor, fuel cell, and hybrid energy storage systems for electric, hybrid electric, fuel cell, and plug-in hybrid electric vehicles: State of the art," *IEEE Trans. Veh. Technol.*, vol. 59, no. 6, pp. 2806–2814, Jul. 2010.
[5] C. C. Chan, A. Bouscayrol, and K. Chen, "Electric, hybrid, and fuel-cell vehicles: Architectures and modeling," *IEEE Trans. Veh. Technol.*, vol. 59, no. 2, pp. 589–598, Feb. 2010.
[6] T. Azib, O. Bethoux, G. Remy, C. Marchand, and E. Berthelot, "An innovative control strategy of a single converter for hybrid fuel cell/supercapacitor power source," *IEEE Trans. Ind. Electron.*, vol. 57, no. 12, pp. 4024–4031, Dec. 2010.
[7] J. Dixon, I. Nakashima, E. F. Arcos, and M. Ortuzar, "Electric vehicle using a combination of ultracapacitors and zebra battery," *IEEE Trans. Ind. Electron.*, vol. 57, no. 3, pp. 943–949, Mar. 2010.
[8] M. B. Camara, H. Gualous, F. Gustin, A. Berthon, and B. Dakyo, "DC/DC converter design for supercapacitor and battery power management in hybrid vehicle applications-polynomial control strategy," *IEEE Trans. Ind. Electron.*, vol. 57, no. 2, pp. 587–597, Feb. 2010.
[9] E. Vinot, R. Trigui, and B. Jeanneret, "Optimal management of electric vehicles with a hybrid storage system," in *Proc. IEEE Veh. Power Propulsion Conf.*, 2010, pp. 1–6.
[10] R. de Castro, P. Melo, P. Pacheco, R. E. Araujo, and D. Freitas, "A control allocation approach to manage multiple energy sources in EVS," in *Proc. IEEE VPPC*, 2011, pp. 1–6.
[11] J. Moreno, M. E. Ortuzar, and J. W. Dixon, "Energy-management system for a hybrid electric vehicle, using ultracapacitors and neural networks," *IEEE Trans. Ind. Electron.*, vol. 53, no. 2, pp. 614–623, Apr. 2006.
[12] A. L. Allegre, A. Bouscayrol, and R. Trigui, "Influence of control strategies on battery/supercapacitor hybrid energy storage systems for traction applications," in *Proc. IEEE VPPC*, 2009, pp. 213–220.
[13] G. Yimin and M. Ehsani, "Parametric design of the traction motor and energy storage for series hybrid off-road and military vehicles," *IEEE Trans. Power Electron.*, vol. 21, no. 3, pp. 749–755, May 2006.
[14] H. Douglas and P. Pillay, "Sizing ultracapacitors for hybrid electric vehicles," in *Proc. 31st Annu. Conf. IEEE Ind. Electron. Soc.*, 2005, pp. 1599–1604.
[15] R. Sadoun, N. Rizoug, P. Bartholomeus, B. Barbedette, and P. Le Moigne, "Optimal sizing of hybrid supply for electric vehicle using li-ion battery and supercapacitor," in *Proc. IEEE VPPC*, 2011, pp. 1–8.
[16] M.-J. Kim and H. Peng, "Power management and design optimization of fuel cell/battery hybrid vehicles," *J. Power Sources*, vol. 165, no. 2, pp. 819–832, Mar. 2007.
[17] A. Ravey, R. Roche, B. Blunier, and A. Miraoui, "Combined optimal sizing and energy management of hybrid electric vehicles," in *Proc. IEEE ITEC Expo*, 2012, pp. 1–6.
[18] O. Sundstrom, L. Guzzella, and P. Soltic, "Torque-assist hybrid electric powertrain sizing: From optimal control towards a sizing law," *IEEE Trans. Control Syst. Technol.*, vol. 18, no. 4, pp. 837–849, Jul. 2010.
[19] N. Murgovski, L. Johannesson, J. Sjöberg, and B. Egardt, "Component sizing of a plug-in hybrid electric powertrain via convex optimization," *Mechatronics*, vol. 22, no. 1, pp. 106–120, Feb. 2012.
[20] R. de Castro, C. Pinto, R. Araújo, P. Melo, and D. Freitas, "Optimal sizing and real time managing of hybrid energy storage systems," in *Proc. IEEE VPPC*, 2012, pp. 321–326.
[21] N. Rizoug, P. Bartholomeus, and P. Le Moigne, "Modeling and characterizing supercapacitors using an online method," *IEEE Trans. Ind. Electron.*, vol. 57, no. 12, pp. 3980–3990, Dec. 2010.
[22] S. Pelissier, "Batteries for electric and hybrid vehicles: State of the art, modeling, testing and aging," in *Proc. Veh. Power Propulsion Conf.*, 2010. [Online]. Available: http://vppc2010.univ-lille1.fr/uploads/PDF/VPPC-10-Pres-tutorial-batteries-Part-II.pdf
[23] C. Mid-Eum, K. Seong-Woo, and S. Seung-Woo, "Energy management optimization in a battery/supercapacitor hybrid energy storage system," *IEEE Trans. Smart Grid*, vol. 3, no. 1, pp. 463–472, Mar. 2012.
[24] R. de Castro, R. Araújo, and D. Freitas, "Wheel slip control of EVS based on sliding mode technique with conditional integrators," *IEEE Trans. Ind. Electron.*, vol. 60, no. 8, pp. 3256–3271, Aug. 2013.
[25] Saft, Nhe 10–100 ni-mh Datasheet, Bagnolet, France 2011.
[26] Maxwell, K2 Series Ultracapacitors Datasheet, San Diego, CA, USA 2012. [Online]. Available: http://www.maxwell.com/products/ultracapacitors/docs/k2series_ds_1015370-4.pdf
[27] G. Souffran, L. Miegeville, and P. Guerin, "Simulation of real-world vehicle missions using a stochastic Markov model for optimal powertrain sizing," *IEEE Trans. Veh. Technol.*, vol. 61, no. 8, pp. 3454–3465, Oct. 2012.
[28] L. Tae-Kyung, B. Adornato, and Z. S. Filipi, "Synthesis of real-world driving cycles and their use for estimating PHEV energy consumption and charging opportunities: Case study for midwest/U.S," *IEEE Trans. Veh. Technol.*, vol. 60, no. 9, pp. 4153–4163, Nov. 2011.
[29] A. Ravey, N. Watrin, B. Blunier, D. Bouquain, and A. Miraoui, "Energy-source-sizing methodology for hybrid fuel cell vehicles based on statistical description of driving cycles," *IEEE Trans. Veh. Technol.*, vol. 60, no. 9, pp. 4164–4174, Nov. 2011.
[30] M. Eshani, Y. Gao, S. Gay, and A. Emadi, *Modern Electric, Hybrid Electric and Fuel Cell Vehicles*. Boca Raton, FL, USA: CRC, 2005.
[31] D. Graovac, M. Prschel, and A. Kniep, Mosfet Power Losses Calculation Using the Datasheet Parameters, Infineon Technologies AG, Neubiberg, Germany 2006.
[32] M. Kabalo *et al.*, "Experimental validation of a high-voltage-ratio low input current ripple converters for hybrid fuel cell supercapacitors systems," *IEEE Trans. Veh. Technol.*, vol. 61, no. 8, pp. 3430–3440, Oct. 2012.
[33] O. Hegazy, J. Van Mierlo, and P. Lataire, "Analysis, modeling, and implementation of a multidevice interleaved DC/DC converter for fuel cell hybrid electric vehicles," *IEEE Trans. Power Electron.*, vol. 27, no. 11, pp. 4445–4458, Nov. 2012.
[34] S. Lim and K. Nam, "Loss-minimising control scheme for induction motors," *Proc. Inst. Elect. Eng.—Elect. Power Appl.*, vol. 151, no. 4, pp. 385–397, Jul. 2004.
[35] F. Casanellas, "Losses in PWM inverters using IGBTs," *Proc. Inst. Elect. Eng.—Elect. Power Appl.*, vol. 141, no. 5, pp. 235–239, Sep. 1994.
[36] L. Guzzella and A. Amstutz, *The QSS Toolbox Manual*. Zurich, Switzerland: ETH Zurich, 2005, [Online]. Available: http://www.idsc.ethz.ch/Downloads/DownloadFiles/qss/index
[37] C. R. Akli, X. Roboam, B. Sareni, and A. Jeunesse, "Energy management and sizing of a hybrid locomotive," in *Proc. Eur. Conf. Power Electron. Appl.*, 2007, pp. 1–10.
[38] J. Curti, X. Huang, R. Minaki, and Y. Hori, "A simplified power management strategy for a supercapacitor/battery hybrid energy storage system using the half-controlled converter," in *Proc. 38th Annu. Conf. IEEE Ind. Electron. Soc.*, 2012, pp. 4006–4011.
[39] S. Boyd and L. Vandenberghe, *Convex Optimization*. Cambridge, U.K.: Cambridge Univ. Press, 2004.
[40] R. Fourer, D. Gay, and B. Kernighan, *AMPL: A Modeling Language for Mathematical Programming*. Pacific Grove, CA, USA: Brooks/Cole, 2003.
[41] D. M. Gay, *Automatic Differentiation of Nonlinear AMPL Models*. Philadelphia, PA, USA: SIAM, 1991.
[42] A. Wachter and L. T. Biegler, "On the implementation of a primal-dual interior point filter line search algorithm for large-scale nonlinear programming," *Math. Programm.*, vol. 106, no. 1, pp. 25–57, May 2006.
[43] T. J. Barlow, S. Latham, I. S. McCrae, and P. G. Boulter, "A reference book of vehicle driving cycles for use in the measurments of road vehicles emissions," TRL Limited, Berkshire, U.K., Tech. Rep., 2009.

Rui Esteves Araújo (M'97) was born in Viana do Castelo, Portugal, in 1964. He received the Electrical Engineering, M.Sc., and Ph.D. degrees from the University of Porto, Porto, Portugal, in 1987, 1992, and 2001, respectively.

From 1987 to 1988, he was an Electrotechnical Engineer with the Project Department, Adira Company, Porto, and from 1988 to 1989, he was a Researcher with the Institute for Systems and Computer Engineering Technology and Science (INESC TEC), Porto. Since 1989, he has been with the University of Porto, where he is currently an Assistant Professor with the Department of Electrotechnical and Computer Engineering, Faculty of Engineering. He has also been with INESC TEC since April 2010, where he is currently a Researcher with the Power Systems Unit. He is the author of over 50 technical papers and and a holder of one patent. His teaching interests include power electronics, electrical machines, and drives. He is a Consultant with the European Commission Framework Programmes. He has coordinated two national research projects. His contributions are focused in the field motion control for industrial, electrical vehicle, and automotive applications. His research interests include energy efficiency in electric machines, design and control of power converters, industrial electronics applications to distributed power generation systems based on renewable energy, and motion control applied to electric vehicles.

Ricardo de Castro (S'09–M'13) was born in Porto, Portugal, in 1983. He received the Licenciatura and Ph.D. degrees in electrical and computer engineering from the University of Porto, in 2006 and 2013, respectively.

From 2007 to 2008, he was an Entrepreneur with the WeMoveU project, targeting the development of powertrain control solutions for light electric vehicles. Since 2013, he has been a Researcher with the Institute of System Dynamics and Control, German Aerospace Center, Wessling, Germany. His research interests include vehicle dynamics, tire–road friction estimation, and battery–supercapacitor hybridization.

Cláudio Pinto (S'13) was born in Porto, Portugal. He received the B.S. degree in electric engineering and the M.S. degree from the University of Porto, in 2010 and 2012, respectively.

He is currently with the Institute for Systems and Computer Engineering Technology and Science, Porto. His research interests include power electronics, electric vehicles, and energy management of hybrid energy storage systems.

Pedro Melo (S'10) received the Electrical Engineering and M.Sc. degrees from the the University of Porto, Porto, Portugal, where he is currently working toward the Ph.D. degree with the Faculty of Engineering.

Since 2001, he has been an Assistant Professor with the Department of Electrical Engineering, School of Engineering, Polytechnic Institute of Porto. His main research interests include modelation and control of electrical machines, design and materials for high-efficiency machines, and energy management systems for electric vehicles.

Diamantino Freitas was born in Porto, Portugal, in 1954. He received the Electrotechnical Engineering degree and the Ph.D. degree from the University of Porto, Porto, Portugal, in 1976 and 1991, respectively.

In 1974, he joined the Department of Electrotechnical and Computer Engineering, Faculty of Engineering, University of Porto, as a Teaching Assistant and has been an Associate Professor since 2003. From 2003 to 2013, he was a consultant in electroacoustics with the Fatima Shrine, Portugal, and since 2005, he has been the Technical Leader of the NAVMETRO system for guidance of blind persons in the metro transport system of Porto. He participated and coordinated several national and international R&D projects and had been a National Delegate to European COST actions, namely COST 288 and COST 219. He is the author or coauthor of 64 papers published in international conference proceedings with reviewers, six international book chapters, and 17 papers in international journals. He has received one patent at the national and international level. His research interests include applications of electronics and signal processing, particularly on electroacoustics, system identification/modeling/control, automatic speech processing, accessibility for persons with special needs, biomedical engineering, and rehabilitation engineering.